Acta Cryst. (1990). A46, 594-606

Surface Phenomena in RHEED and REM

BY Y. MA* AND L. D. MARKS

Materials Research Center, Northwestern University, Evanston, IL 60208, *USA*

(*Received* 19 *July* 1989; *accepted* 22 *February* 1990)

Abstract

Based upon previous results for the Bloch-wave solution in the Bragg case and the consistency between the Bloch-wave solution and multislicing in the Bragg case, a complete numerical solution has been developed for reflection electron diffraction called the Bloch wave and multislice combined for reflection (BMCR) method. Results are presented of applying the BMCR method to several problems in high-energy electron reflection. First, simulations of the effects of surface reconstruction and adsorption on RHEED patterns are reported. Next, the results of simulations of surface steps are shown and their effects on the wave field analyzed numerically. Last, the existence of the surface wave which is related to electron surface resonance phenomena is demonstrated.

I. Introduction

RHEED (reflection high-energy electron diffraction) is a well established technique in surface science. It is especially useful for the identification of surface crystallization, reconstruction and relaxation *etc.* (Menadue, 1972; Daimon & Ino, 1985). However, the theoretical development of RHEED has been rather slow, and in general the intensity in the diffraction pattern cannot be subjected to analysis and only the positions of the spots are used for structural identification. It is clear that RHEED patterns contain far more information than just the position of the spots, but analyzing this information relies heavily on the development of a dynamical electron reflection theory.

Miyake & Hayakawa (1966) clearly indicated that there was strong evidence that electron reflection in both low-energy and high-energy cases is dynamical. Even for the low-energy case, interference between different beams was widely observed in LEED (low-energy electron diffraction) patterns and intensity profiles and the concept of a thin penetration depth are only meaningful in some restricted cases.

Direct and localized observation of surfaces has been attempted for a long time with increasing interest in surface science, while various techniques, such as LEED, RHEED, Auger-electron spectroscopy AES and photoemission spectroscopy (XPS, UPS), unfortunately can only provide average statistical information. The spatial resolution of various microprobe analysis techniques such as AES, XPS and UPS is limited by the probe size and energy dissipation. Therefore, making use of reflected electrons to image surfaces is a logical and natural step.

Many authors have made significant contributions to the development of dynamical theory in electron reflection. The Bloch-wave theory was first developed in this field by Bethe (1928), Kato (1952), Miyake, Kohra & Takagi (1954), Whelan & Hirsch (1957), Fujimoto (1959), Kohra, Moliere, Nakano & Ariyama (1962), Colella (1972), Moon (1972) and Britze & Meyer-Ehmsen (1978). Later, a multislice method (slices parallel to the surface) was developed by Maksym & Beeby (1981, 1982) and Ichimiya (1983) for electron reflection. More recently, Zhao, Poon & Tong (1988) and Zhao & Tong (1988) developed an invariant-embedding R-matrix scheme for calculating a rocking curve in RHEED. All of these approaches focus on the diffraction aspect of the problem and an analysis in real space of these methods has not been reported. In 1986, Peng & Cowley subjected the problem to both real- and reciprocal-space analyses by utilizing a multislice method with slices perpendicular to the surface, which was initialized by the revival of the REM (reflection electron microscopy) technique in electron microscopes. The advantage of this method is its flexibility for simulating various surface structures. However, a problem is serious edge effects, which makes stationary solutions hard to achieve.

We have analyzed the Bloch-wave solution in a semi-infinite crystal in the Bragg case (Marks & Ma, 1988, 1989*a*; Ma & Marks, 1989) and the consistency between the solution and its propagation *via* multislice iterations (Ma & Marks, 1990). The results have clearly shown that consistency has been reached with sufficient numerical accuracy, and a stationary solution for a free surface achieved with the edge effects reduced to the level which permits simulations of surface phenomena in a manageable and reliable manner. This means that a new method which we call Bloch wave and multislice combined for reflection (the BMCR method) has emerged. It combines the advantages of the Bloch-wave method and the multislice approach (stationary solution obtainable for the

* Present address: Department of Materials Science and Engineering, University of Utah, Salt Lake City, UT 84112, USA.

0108-7673/90/070594-13$03.00

former and flexibility of imperfect-surface simulation for the latter) and reduces the effects of the disadvantages of both (inflexibility of imperfect-surface simulation for the former and edge effects for the latter). In this paper, we report results of simulating several surface phenomena, *i.e.* stationary solutions in the crystal potential with different non-free surfaces using the BMCR method.

We report the simulation of the effects of surface reconstructions and adsorption on RHEED patterns, which has been discussed in part in a previous paper (Marks & Ma, 1990). Surface reconstructions and adsorption are well known and experimentally well studied surface phenomena in RHEED. Next, we present simulations of surface steps and analyze their effects on the wave field numerically. Finally, we demonstrate the existence of a surface wave which is related to surface resonance phenomena.

II. Surface reconstruction and adsorption in RHEED

In this section we present the results of dynamical simulations of a surface reconstruction and adsorption in RHEED by using the newly developed BMCR method. Fig. 1 shows the unit cell for the Bloch-wave calculation in (*a*) and the multislice iterations in (*b*). The system used is f.c.c. gold and the absorption is included by taking the imaginary potential as 10% of the real potential in both the Bloch-wave and multislice calculations. The size of the two unit cells is $8a \times 2a$ (a denotes the magnitude of the primitive unit-cell vector of gold). For the 2×1 reconstruction or adsorption, the y dimension of the unit cell needs to be two times larger than the primitive vector. As far as the requirement of the sampling theorem is satisfied and the maximum array size allowed in the programming is used, the maximum x dimension of the unit cell is $8a$. This may result in more serious edge effects during the multislice iterations. Here, 'edge effects' refer to the edge of the tilted incident wave field moving towards the surface during the multislice iteration. This is because a sampling array with finite size in the multislice iteration is implicitly periodically repeated and therefore fails at one edge to model correctly the infinite incidence wave. To reduce the edge effects, the surface is moved further towards the right-hand side in each unit cell as indicated in both Figs. 1(*a*) and (*b*), which leaves more room for the reflected waves. This is feasible because, when absorption is included, the extreme low intensity deep in the crystal damps edge effects on the right-hand side. The sampling array is 512×128. The coordination in the calculation is set up as the following: the z axis [001] is from the left side to the right pointing inward to the crystal; the x axis [100] points up to down and the y axis [010] is inwardly normal to the page. The y axis is along the forward direction of the incident wave. All calculations in this paper were performed for 100 keV incident electrons.

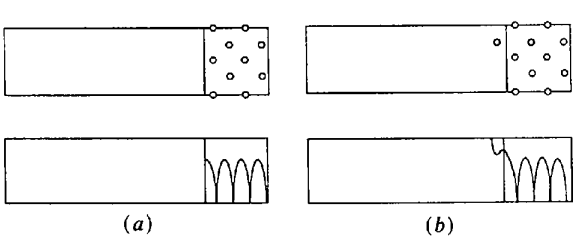

Fig. 1. Unit-cell set up for the simulation of surface reconstruction and adsorption. (*a*) Unit cell for the Bloch-wave calculation. (*b*) Unit cell for multislice calculation. The unit-cell size is $8a \times 2a$, $a = 4{\cdot}0497$ Å.

For the 2×1 gold-surface reconstruction, one Au atom is placed on the site indicated in (*b*) for each of four slices with no relaxation. For a 2×1 chemisorbed oxygen surface, the Au atom was replaced by an O atom. The position of the surface in each slice is indicated in Fig. 1, at (3/4, 0) if the left end of each slice is taken as (0, 0), *i.e.* three quarters of the horizontal axis towards the right side of each slice. The first 50–100 slices are for a flat surface so that the incident or trial wave function converges to the true solution for the free surface.

Fig. 2 shows outputs of the wave fields from multislice iterations for the 2×1 gold reconstruction in (i) and 2×1 oxygen adsorption in (ii). If the thickness of the first, (*a*), is taken as the reference thickness of the calculation, 0 Å, the thickness of the last slice (*l*) is 556·8 Å. The thickness difference between any two adjacent slices is 50 Å and the incidence angle is 30 mrad. The first slice is the solution of the Bloch-wave calculation. The position of the surface of each slice is as indicated in Fig. 1: (3/4, 0). As expected, the figure shows that the wave disturbance for the 2×1 gold reconstruction is much stronger than that for 2×1 oxygen adsorption. The incident wave starts to be scattered by the surface atoms at the third slice. In subsequent slices, the incident wave appears to be scattered at the lower atom position, even though there is no atom on that site. This looks like a 'mirror effect' and is clearer when the incident wave is excluded and only the Bragg reflected waves are present, as shown in Fig. 3. The slices in Fig. 3 correspond to the outputs in Fig. 2. The size of each slice in Fig. 3 is $4a \times 2a$. Each slice in Fig. 3 extends from the surface into the vacuum (from right to left) a distance of 16·2 Å as indicated in the figure.

The edge effects in Fig. 2 appear quite serious [the edge of the incident wave field on the left side almost moves into the crystal surface at the last slice (1)] because the size of the unit cell is limited by the maximum sampling array. The Bragg reflected wave fields in slices *i* to *l* of Fig. 3 show the same effects. This will erode the accuracy of the numerical investigations in the Bragg reflected wave fields and the calculation would lose reliability when the incident edge moves into the crystal, because it is no longer a stationary solution.

Fig. 4(i) shows the Bragg reflected waves in reciprocal space, *i.e.* the RHEED patterns excluding the incidence beam, in which each pattern corresponds to the slice in Fig. 3(i) labeled with the same letter. Fig. 4(ii) is a convergence analysis of Fig. 4(i) (Ma & Marks, 1990). Fig. 5 corresponds to Fig. 3(ii). The convergence analyses for both Figs. 4(i) and 5(i) show stability after 300 Å.

To display the patterns more clearly, Fig. 6 shows the y-modulated patterns (the intensity of each pattern is presented in the third dimension) of (a) and (l) for both Figs. 4(i) and 5(i). There are several points to note in Fig. 6:

(i) (01) and ($0\bar{1}$) forbidden Bragg spots emerge at 556·8 Å because of the existence of the 2×1 surface adatoms.

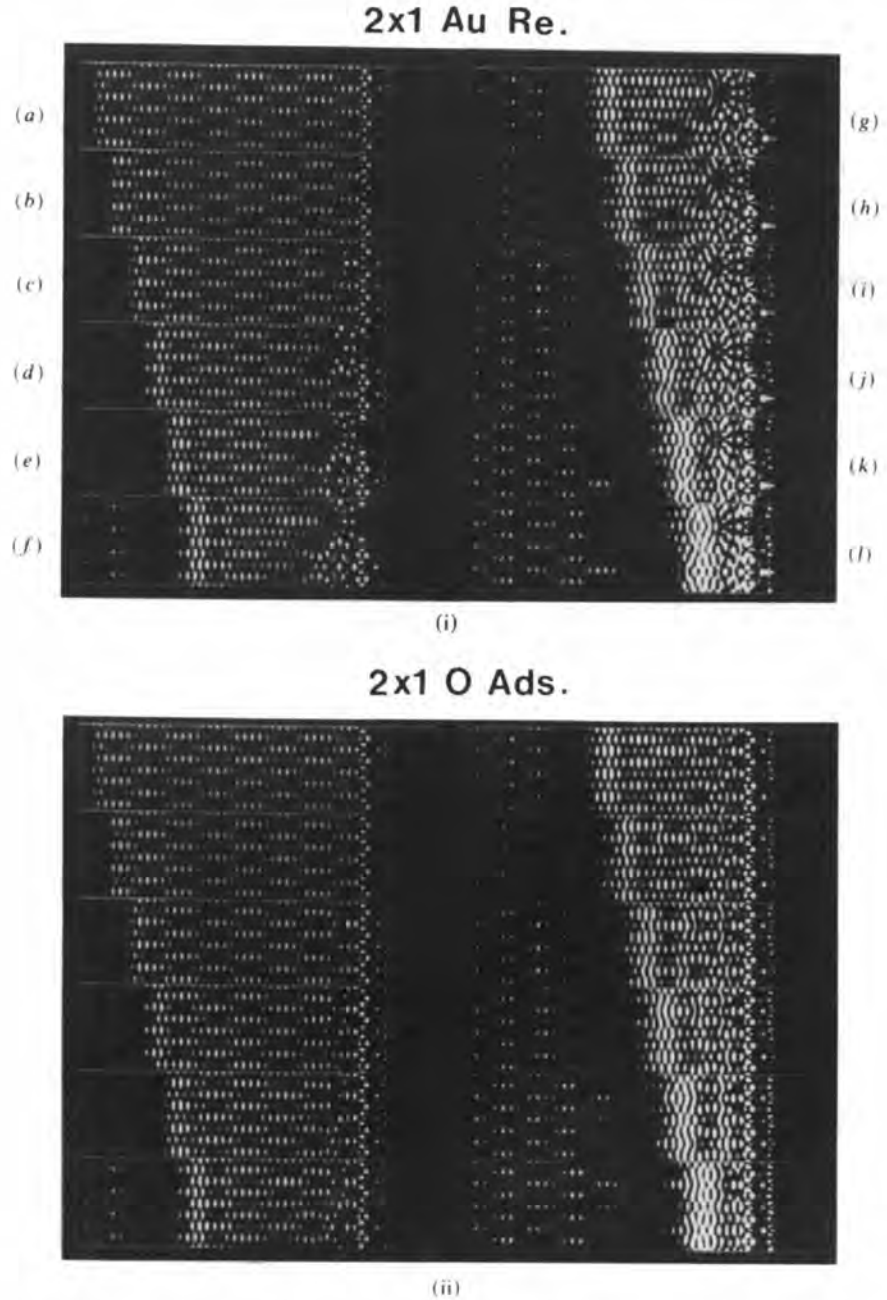

Fig. 2. Outputs of the wave fields from multislice iterations for 2×1 gold reconstruction (i) and 2×1 oxygen adsorption (ii). The thicknesses of the first and last slices are 0 and 556·8 Å respectively. The thickness difference between two nearest slices $\Delta t = 50$ Å, the size of the unit cell in the calculations is $8a\times2a$, with an absorption of 10% and a beam incidence of 30 mrad.

(ii) 2×1 reconstruction spots occur between the Bragg spots. It should be noted that a simulated RHEED pattern for surface reconstruction has never been obtained by the Bloch-wave method or multislice approach individually. The BMCR method demonstrates its advantages on this point.

(iii) The intensities of the reconstruction spots for 2×1 gold are noticeably stronger than for 2×1 oxygen.

(iv) The intensities of the Bragg spots (03) and $(0\bar{3})$ are noticeably stronger than the Bragg spots (01) and $(0\bar{1})$ and the reconstruction spots.

(v) The intensity of the specular spot for 2×1 gold ($t=556{\cdot}8$ Å) is reduced significantly, compared to that for a perfect flat surface ($t=0$ Å), while the intensity of the specular spot for 2×1 oxygen adsorption ($t=556{\cdot}8$ Å) does not change noticeably. This can be explained by dynamical interaction between the different reflected beams caused by the scattering from the adatoms on the surface. The stronger potential scatters more electrons of the specular beam into the Bragg reflected beam. This kind of information can be directly used to analyze experimental data in RHEED.

III. Surface steps

Investigation of surface step distributions in real space can provide useful information with respect to crystal growth, evaporation, surface phase transformations and mechanical properties (Somorjai, 1981). Many different explanations have been proposed for the mechanism of step contrast. Cowley & Peng (1985) considered steps as phase objects with phase contrast arising due to defocusing, deviation from the Bragg condition and possible displacements of the

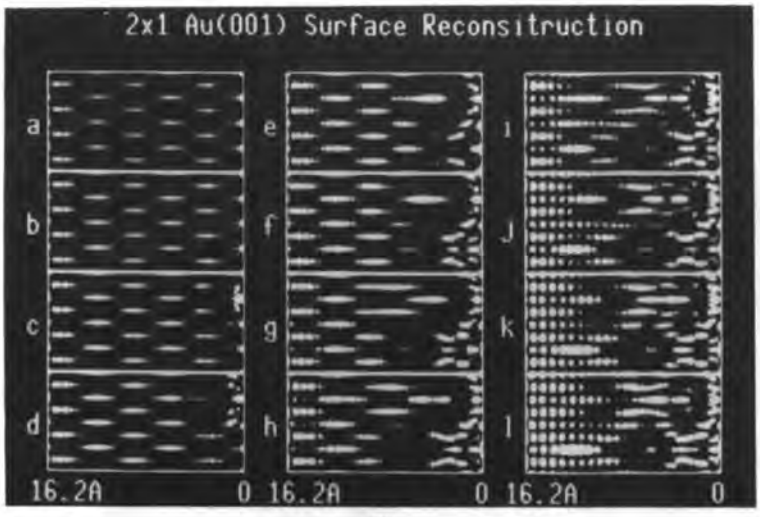

(i)

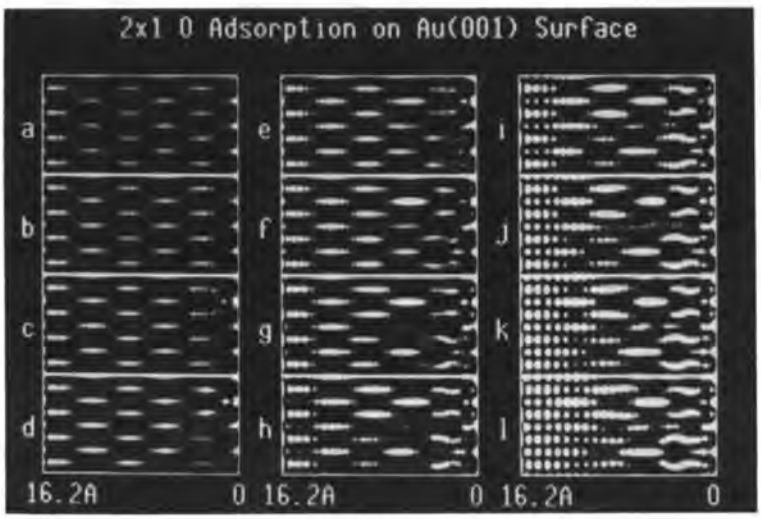

(ii)

Fig. 3. Outputs of the Bragg reflected wave fields, excluding the incident wave, from the multislice iterations, for (i) 2×1 gold reconstruction and (ii) 2×1 oxygen adsorption. The rest of the conditions are the same as in Fig. 2. The thickness series from (*a*) to (*l*) is: 0·0, 50·6, 101·2, . . . , 556·8 Å.

objective aperture, while Turner & Cowley (1981) suggested that a surface step can split the electron beam into Bragg-Bragg (*BB*) and Bragg-Laue (*BL*) beams and the interference between the two produces fringes along the step.

A dynamical interpretation of the step contrast was first attempted by Peng & Cowley (1986) using a multislice approach. However, the calculations were performed without clear evidence that the solution was stationary. Here, we use the BMCR method to simulate surface steps.

Fig. 7 shows the unit-cell constructions of a step up (*a*) and a step down (*b*). The system in the calculation is f.c.c. gold, and absorption is included by taking the imaginary potential as 10% of the real potential in both the Bloch-wave calculation and the multislice calculations. The size of unit cell in the calculations is $16a \times 1a$, while the results are displayed as $8a \times 2a$ and the sampling array is 1024×64. The coordination system used is the same as that in § II. For an atomic step up, one layer of Au atoms is added to the surface. Conversely, for an atomic step down, the outermost layer of Au atoms is taken away from the surface. The first 100 slices were used to achieve a steady wave field in the crystal potential for a free surface without surface truncation. The remaining 400 slices are inserted with a step. Here, only one step is analyzed.

Figs. 8 and 9 show the results of the calculations with surface steps. The total thickness in each case is 607·5 Å, and the thickness difference between the two nearest slices is 50 Å. Fig. 8 shows the results for 25 mrad incidence and Fig. 9 for 30 mrad incidence for both step up (i) and step down (ii). One of the most important features of these results is that the wave fields converge to the original stationary state after about 250 Å (from *d* to *h*), during which the wave fields are disturbed by the steps. In other words, the transition range of 200–250 Å both begins and ends with a stationary state. The results clearly indicate that the simulation of the wave disturbance resulting from the steps has not been affected by edge effects after 607·5 Å iterations, which is a necessary

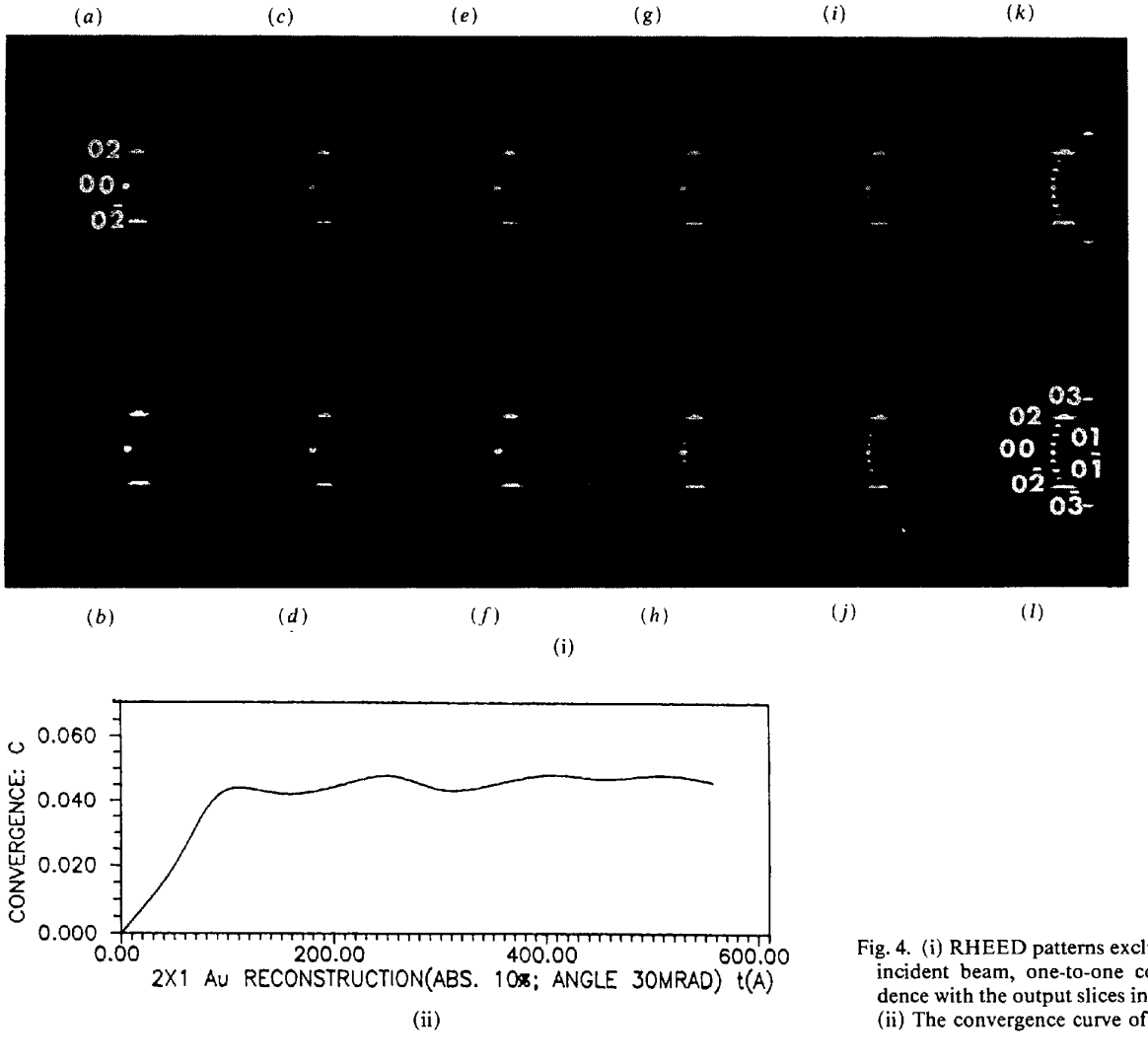

Fig. 4. (i) RHEED patterns excluding the incident beam, one-to-one correspondence with the output slices in Fig. 2(i). (ii) The convergence curve of (i).

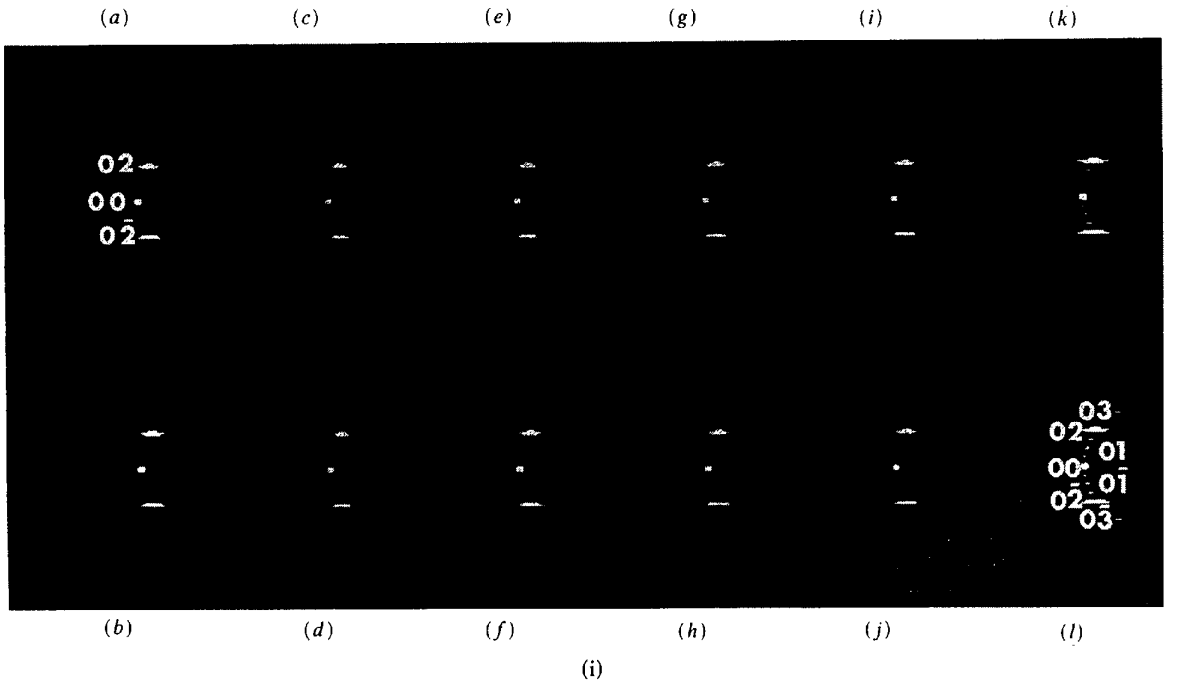

Fig. 5. (i) RHEED patterns excluding the incident beam, one-to-one correspondence with the output slices in Fig. 2(ii). (ii) The convergence curve of (i).

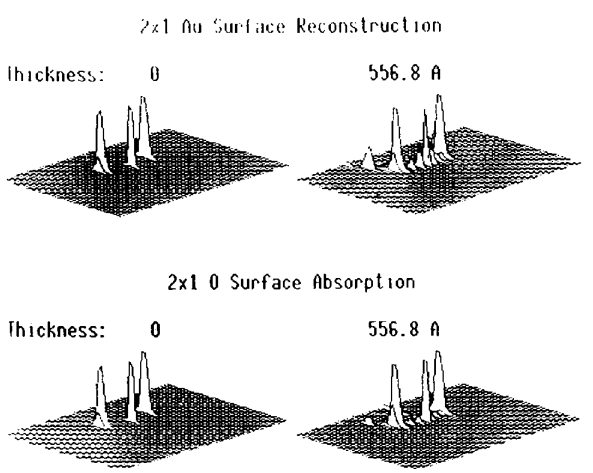

Fig. 6. y-modulated patterns of (a) and (l) of Figs. 4(i) and 5(i).

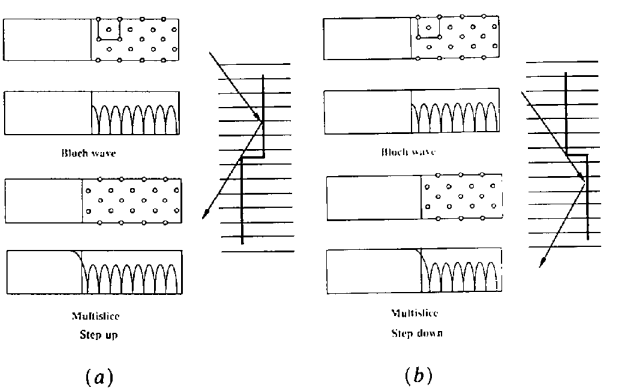

Fig. 7. Unit-cell set up for simulations of (a) step up and (b) step down. The upper two are the unit cells for the Bloch-wave calculation and the lower two are the unit cells for multislice iterations. The size of the unit cell in the calculations is $16a \times 1a$ ($a = 4{\cdot}0497$ Å), and the wave fields are displayed as $8a \times 2a$.

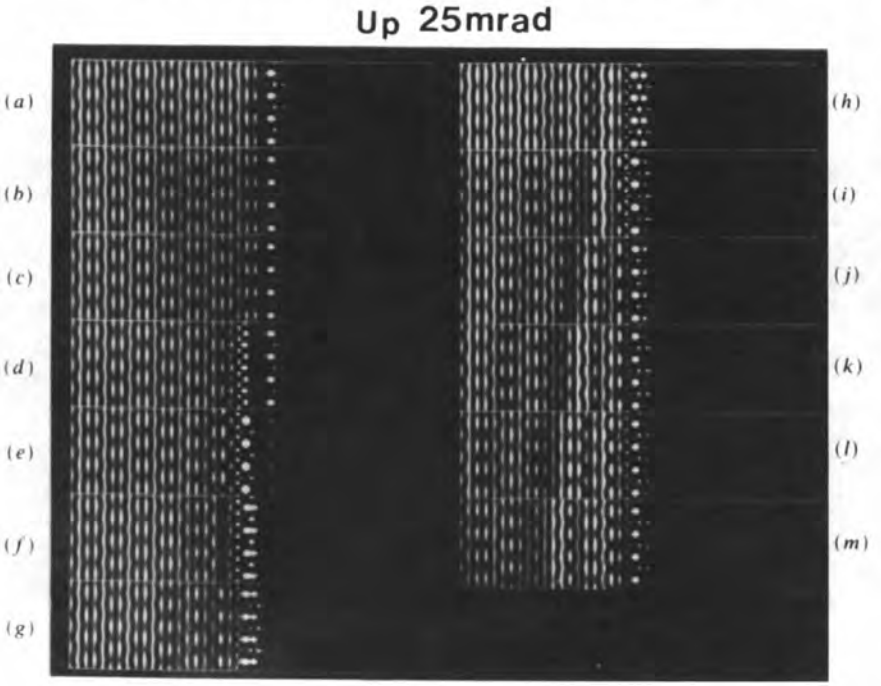

(i)

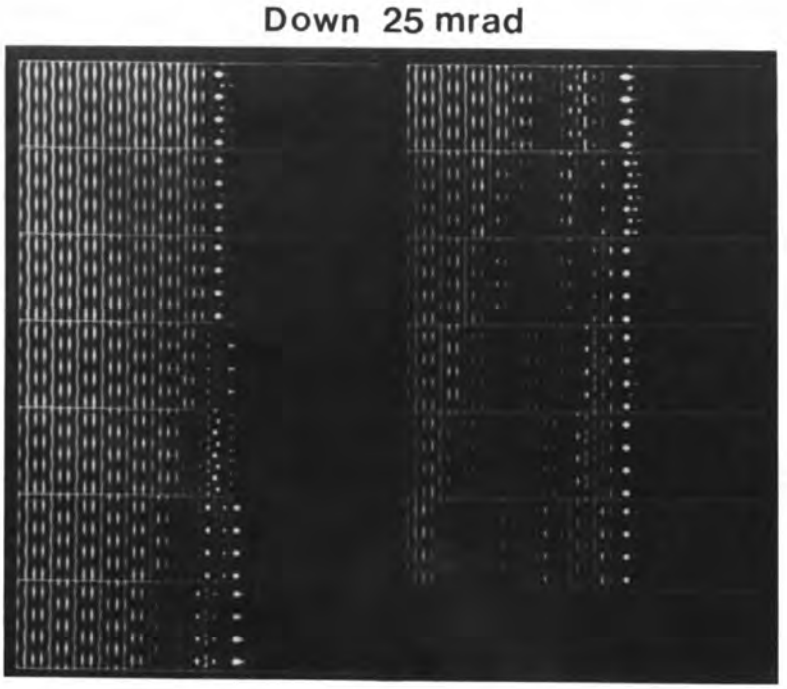

(ii)

Fig. 8. Outputs of the wave field from multislice iterations for the simulations of (i) step up and (ii) step down. The thicknesses of the first and last slices are 0 and 607·5 Å respectively. The thickness difference between two nearest slices is 50 Å, the size of unit cell in the calculation is $16a \times 1a$, the size of unit cell displayed is $8a \times 2a$ with an absorption of 10%. The beam incidence is 25 mrad. The step is introduced at $t = 101{\cdot}2$ Å.

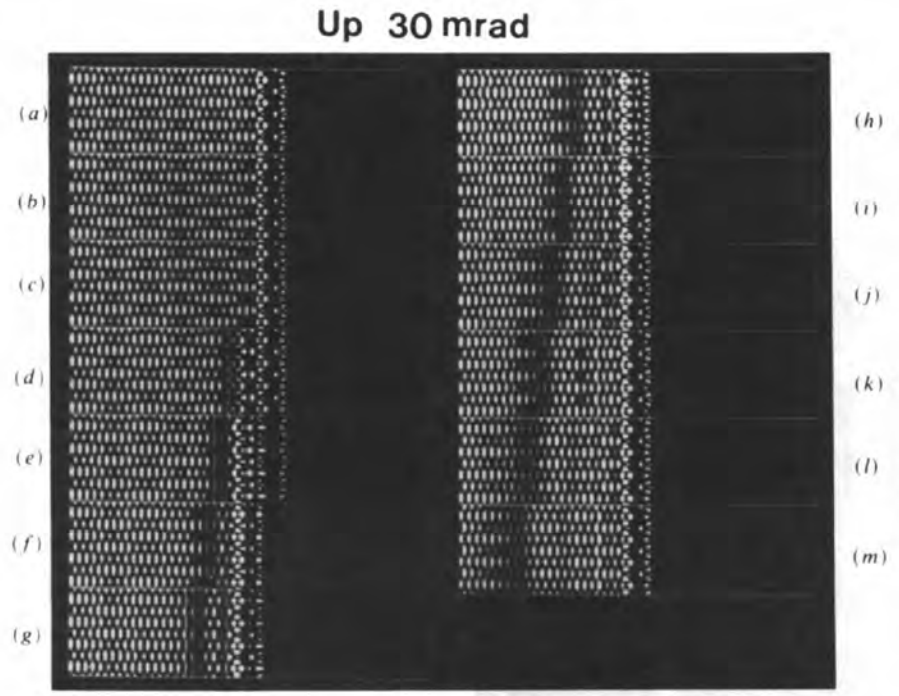

(i)

(ii)

Fig. 9. Outputs of wave field from multislice iteration under the same conditions as for Fig. 8, except for beam incidence of 30 mrad.

condition for the validity of the analysis. Comparing (i) and (ii) in both Figs. 8 and 9, one can easily find that the wave disturbance of a step up is better confined than that of step down and the transition range of a step up (about 250 Å) is a little shorter than that of a step down (>250 Å). This phenomenon so far has no experimental confirmation.

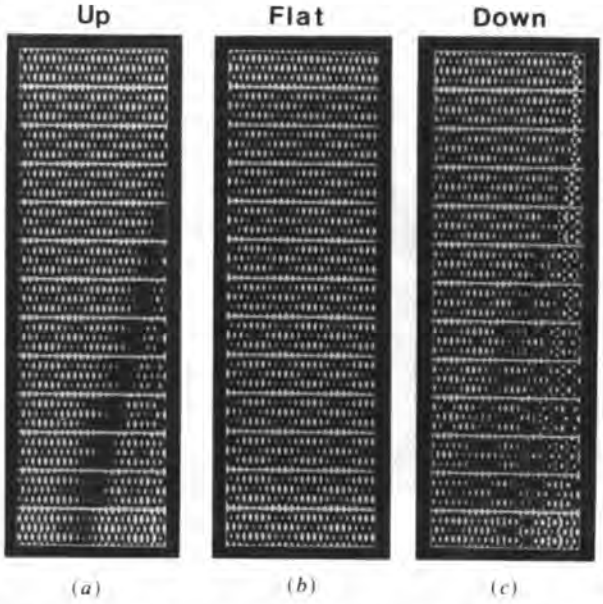

Fig. 10. Outputs of the wave fields in vacuum which include the Bragg reflected waves and the incident wave from multislice iteration for the simulations of the surfaces with (*a*) step up, (*b*) flat surface and (*c*) step down. The total thickness is 556·8 Å. The thickness difference between two nearest slices is 50 Å, the size of unit cells displayed is $4a \times 1a$, extending from surface (right side) into vacuum (left side) with an absorption of 10% and the beam incidence is 30 mrad.

For comparison, Fig. 10 shows the wave fields in vacuum for the surface with one step up (*a*), the flat surface (*b*) and the surface with one step down (*c*). The size of each slice displayed is $4a \times 1a$, which extends from surface (origin) into vacuum (from right to left) for a distance of 4*a*. The Bragg reflected wave field excluding the incidence wave is shown in Fig. 11, which corresponds to Fig. 10, except that the size of the displayed slices is $8a \times 1a$, *i.e.* twice as large as that in Fig. 10 along the *z* axis (see Fig. 1). The wave disturbance due to the step appears clearer in Fig. 11, and the electron intensity distribution for a step down appears to be reflected further from the surface than that for a step up.

To simulate REM in an electron microscope, the specular beam was used for imaging and the optical axis tilted to be coincident with the specular beam. One-dimensional images for the last slice in Figs. 10(*a*), (*b*) and (*c*) ($t = 556{\cdot}8$ Å) are shown in Fig. 12(i). These are the plots of wave intensities *versus* the distance extending from the surface into vacuum ($0{\cdot}6 \times 4{\cdot}0497$ Å, from right to left). Each column is a focal series from −3000 to 3000 Å in Figs. 10(*a*), (*b*) and (*c*). The defocus step is 1000 Å. A contrast reversal with defocus is quite clearly demonstrated. However, it should be pointed out that there is a considerable amount of numerical error involved in the calculation due to a limited cell size and the one-dimensional images simulated here should be handled cautiously. For example, the width of each Bragg peak in the *y*-modulated patterns in Fig. 6 indicates the existence of numerical errors.

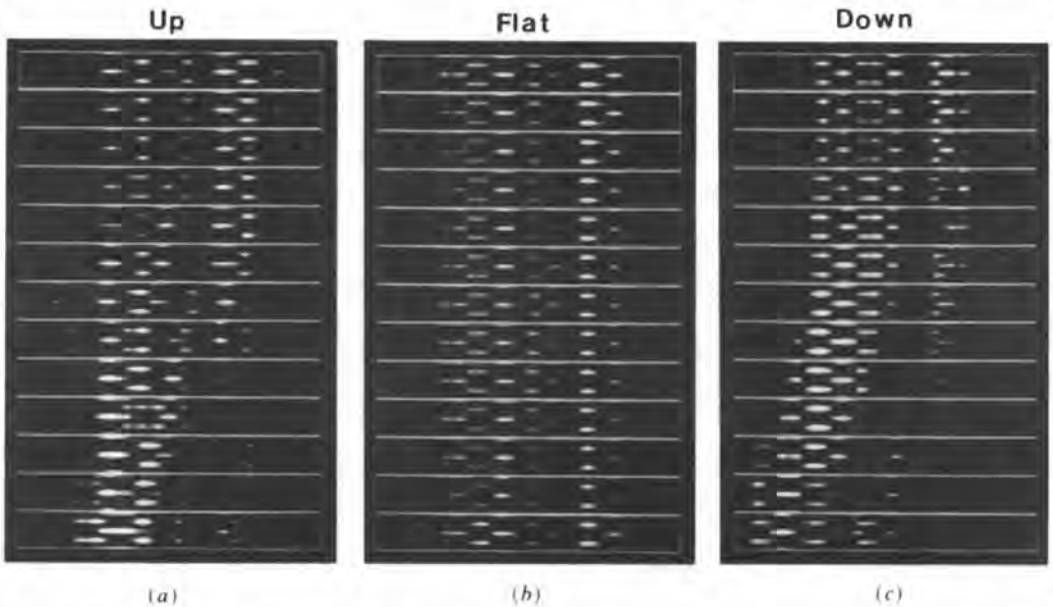

Fig. 11. Outputs of the wave fields excluding the incident beam in vacuum, which corresponds to those in Figs. 9 and 10, except that the size of unit cells displayed is $8a \times 1a$.

Theoretically, all Bragg peaks for an ideal-crystal potential should be narrow and converge to a point and ideally there should be no contrast from the flat surface when a single beam is used. These numerical errors are mainly responsible for the contrast in the images obtained from the free surface. The errors are also involved in the imaging calculation. To partially correct the errors, Fig. 12(ii) shows the results of subtracting the middle column, 1D pictures of the flat surface, from each of the other two columns, 1D pictures of the surfaces with steps. It is obvious that the step contrast is enhanced after the subtraction. To estimate the errors quantitatively, the contrast level of each picture is calculated as CONTRAST = SD/MEAN, where SD is the standard deviation and MEAN is the mean level of the picture. The value of the CONTRAST is averaged over each focal series. For a step up, a flat surface and a step down in Fig. 12(i), we obtained contrast levels from Fig. 12(i) of 0·58, 0·13, 0·31. After the correction, as shown in Fig. 12(ii), we obtained 1·41, 0, 0·87. Obviously, the errors are large: from 22 to 40%. Note that the results suggest that the contrast level of a step up is generally higher than that of a step down.

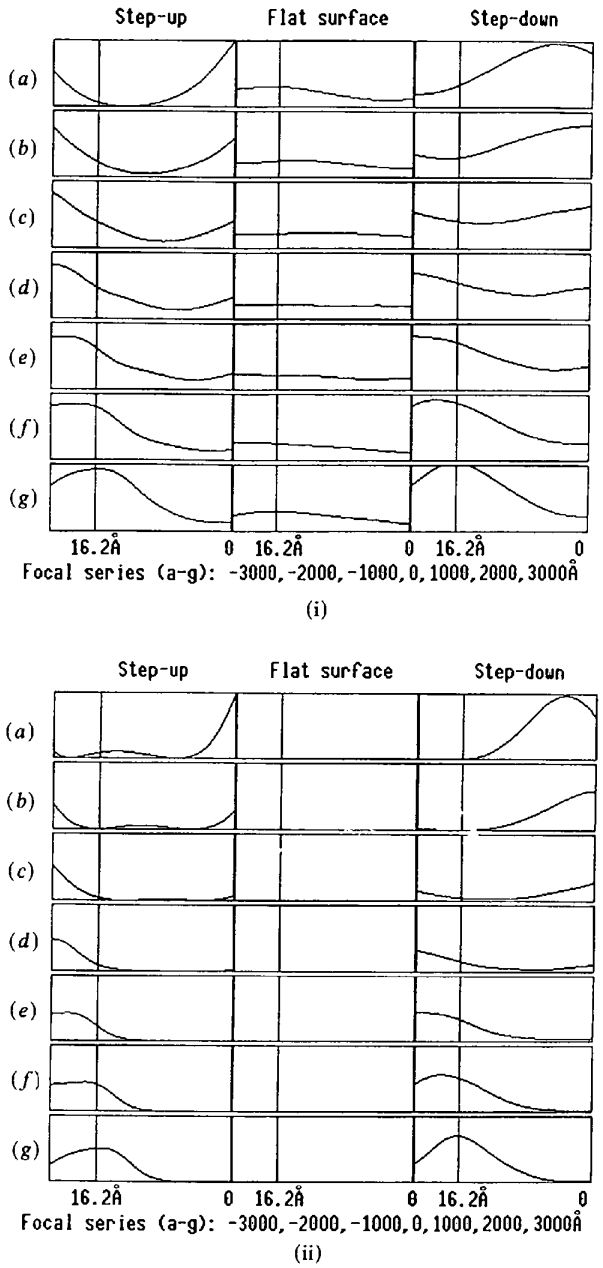

Fig. 12. (i) Focal series of one-dimensional imaging contrasts using the specular beam alone, crossing the wave disturbance caused by steps in the last slice in Figs. 10(*a*), (*b*) and (*c*) ($t = 556{\cdot}8$ Å). The defocus range is from −3000 to 3000 Å and the defocus step is 1000 Å. (ii) Results of subtracting the middle column from each of the three columns in (i).

IV. Surface wave

Surface wave is another unanswered topic with a long history in high-energy electron reflection (HEER). The concept of a surface wave dates back to the time when Kikuchi & Nagawa (1933) first observed an intensity enhancement of the specular spot occurring in RHEED when it overlapped an oblique Kikuchi line, which was called 'second kind of intensity anomaly'. Later on, this was renamed as 'surface resonance', 'surface state resonance', 'Bragg surface state resonance (BSR)' and 'surface monolayer resonance' *etc.* (Many more have been used.) It was Miyake *et al.* (1954) who first raised the concept of 'surface wave' in HEER relevant to the 'surface resonance' phenomenon. The authors pointed out that the enhancement of the specular beam can occur if the incident electrons suffer a Bragg reflection on a certain lattice plane which the authors called 'Bragg reflection in a side direction', provided that the boundary surface is a mirror plane of the crystal lattice. The Bragg reflection is expected to travel almost parallel to the crystal surface. This was further studied by Kohra *et al.* (1962), but no quantitative results were reported.

On the other hand, McRae (McRae, 1966, 1979; McRae & Caldwell, 1976) worked on the resonance phenomena in LEED and proposed two theories for the explanation of resonance; the first one in 1966, the second in the 1970's. The origination of the second is resonance theory in nuclear reactions (Feshbach, 1958) which is quite different from traditional dynamical analysis in electron diffraction which is basically an elastic approach. By reference to resonance theory in nuclear reaction, the authors introduced the concept of a surface wave trapped by a surface state. The key point of the theory is subdivision of the incident energy into the components parallel to the surface and normal to the surface, *i.e.* 2D free-electron description. The forbidden gap in the surface band structure together with the surface

potential barrier are considered to confine electrons in the surface region of the crystal and the surface resonance is explained as the result of the remission of these temporarily trapped electrons back to the vacuum. The concept of 'surface wave trapped in surface state' mixed with that of a 'Bragg reflection in a side direction parallel with the surface' was later inherited or even extended by many authors in HEED (Wang, Lu & Cowley, 1987; Peng & Cowley, 1988).

From our point of view, a consistent, explicit and convincing theory on electron surface resonance phenomena and surface wave, valid for both low- and high-energy cases, has not appeared and the question of consistency between various concepts of 'surface resonance' and 'surface wave' has not been answered. For surface waves, there is no clear experimental confirmation so far.

In this section we present results which clearly indicated the possible existence of a surface wave. However, we do no more than provide a simple presentation of the numerical results and further theoretical speculation has not been attempted.

Fig. 13 shows the y-modulated RHEED patterns at three different thicknesses, 506·2, 556·8, 607·5 Å, for three different surfaces: a surface with a step up, a flat surface and a surface with a step down. The incident angle is 35 mrad and the treatment of absorption is the same as that for Fig. 7. The steps are introduced at 101·2 Å. It should be noted that the threshold incidence for the emergence of the (04) spots, in the case of 100 keV electrons and a gold (001) surface, is 36·6 mrad, which is close to 35 mrad. The spots in the flat-surface patterns are well defined and there are not many additional features. However, the patterns from the surfaces with steps appear quite different from those for a flat surface, although the positions of the three basic Bragg reflection spots remained unchanged. It should be pointed out that there is no intensity comparison between the results from two different surfaces, because of different normalization and displaying conditions.

For the patterns of the surface with a step up, spot broadening is apparent. The broadening of beams caused by surface features in the Bragg case is similar to the broadening in transmission caused by defects in the bulk crystal in the Laue case, which is a well accepted and understood phenomenon. More interestingly, all of the three Bragg reflected beams have a small satellite beam. We have discussed the correlation between spot splitting and regular surface steps elsewhere (Marks & Ma, 1989*a*) by using a Bloch-wave argument alone. Here, the results of the BMCR method also indicate splitting from a single step. In each pattern of the surface with a step down, two additional spots occur near the intersections between the Laue circle and the x axis in reciprocal space. These two beams are apparently parallel or nearly parallel to the surface. It is obvious that these two spots are the results of a step down if one compares the patterns to the patterns from the flat surface and the surface with a step up. This also shows that the idea that the step down may make the surface wave more visible is logical and comprehensive. However, the true physical mechanism of the emergence of these spots merits further study and a clear experimental conformation is needed for the understanding of a 'surface wave' and its correlation with 'surface resonance' phenomena. Nevertheless, theoretical speculation of the existence of a surface wave, which is either a 'Bragg reflection in side direction' in the sense of Miyake *et al.* (1954) or a 'wave trapped in surface state' in the sense of McRae (1979), is not necessarily related to steps or other surface features. Therefore, there should also be additional spots along

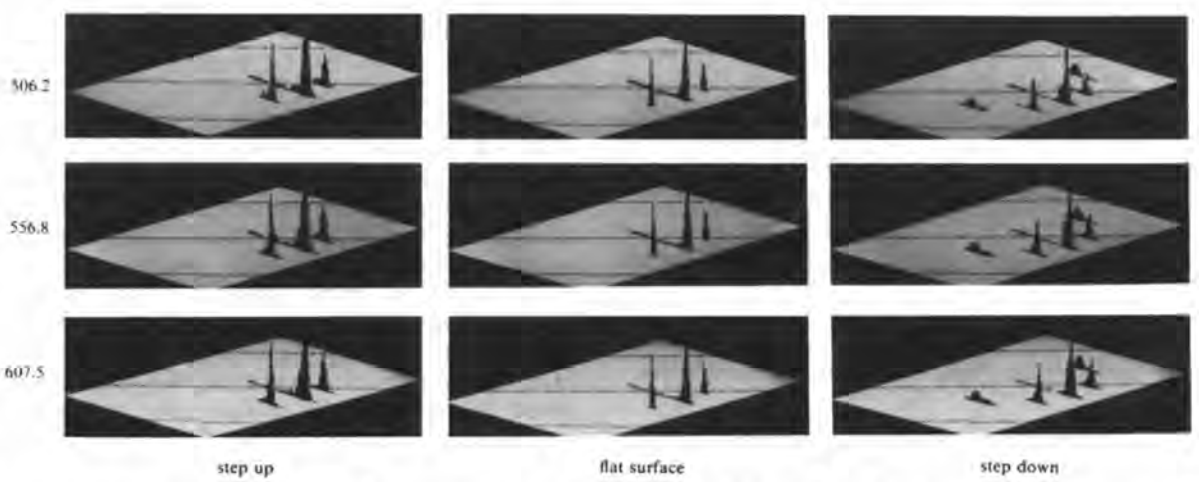

Fig. 13. y-modulated diffraction patterns at three different thicknesses, 506·2, 556·8, 607·5 Å, for three different surfaces, surface with step up, flat surface and surface with step down. The beam incidence is 35 mrad and absorption 10%. The step is introduced at $t = 101{\cdot}2$ Å.

the x axis in the patterns of the flat surface and the surface with a step up. We suspected that the intensities of these spots are extremely low and so are difficult to see when with other spots. We have displayed these regions separately and tried to detect spots with low intensity. The results are shown in Fig. 14; the spots are there, but they have extremely low intensities, 10^{-4}–10^{-5} lower than the intensities of the spots shown in Fig. 13. Apparently, these waves have no way to emerge in the experiments and will be concealed in the background of inelastic scattering. Fig. 14 shows spots for 'surface waves' in the patterns of the last two output slices, $t = 506{\cdot}2$, $556{\cdot}8$ Å, for the flat surface and the surface with a step up. The contrast ranges for displaying the y-modulated patterns from the two surfaces are the same. The intensities of the surface waves for a flat surface appear weaker than those of the surface with a step up, which implies that the disturbances of a step up or other surface features also tend to 'release' the surface wave.

At this stage of the numerical investigation, we can at least conclude that a 'surface wave' may be a true detectable entity in high-energy electron reflection and the best system for its observation would be an atomic smooth surface with some down steps. The correlation between the existence of 'surface wave' and 'surface resonance' merits further studies.

V. Concluding remarks

The results obtained using the BMCR method in this paper can be considered as the last step of the development of the method; application of the BMCR method to some real problems and testing the potential of the method.

The results clearly indicate that the BMCR method is feasible and reliable. In other words, the 'last step' is also the first step of more applications of the method. The consistency between the Bloch-wave and multislice approaches provides a strong mutual proof of the validity for both approaches in the Bragg case. Their combination, the BMCR method, opens up a new way to exploit the physical processes of electron-crystal-surface collision.

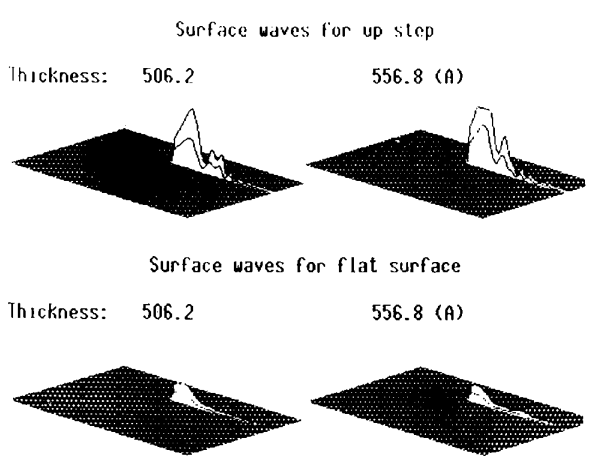

Fig. 14. Spots of surface waves in the patterns of the last two output slices, $t = 506{\cdot}2$, $556{\cdot}8$ Å, for the flat surface and the surface with step up.

The consistency investigation in a previous paper (Ma & Marks, 1990) has indicated that the effects of surface truncation in the Bloch-wave method are small and start to decline after 100 Å. Therefore, we consider that it is reasonable and practical to start simulations of surface features at the thickness of 100 Å, although it is still not a perfectly converged stationary solution in the crystal potential without surface truncation, but this appears to be a surmountable problem.

The computation speed of the BMCR method has been brought up to the speed of the conventional multislice method by using 'side input' of the Bloch-wave function as a top cap. For the simulations of 600 slices of sampling size 1024×64 on an Apollo 3500, the CPU time does not exceed 6 h. This is manageable on many computation facilities.

However, the BMCR method does not mean the elimination of edge effects (Fig. 2). For the multislice iterations with a non-periodic crystal potential, edge effects will always be there. We should mention that we have recently tested the edge-patching method mentioned in a previous paper (Ma & Marks, 1990), and preliminary results indicate that it can significantly reduce the edge effects and improve the stationary solution. This will be discussed elsewhere (Ma, 1990).

It appears that the BMCR method does provide a reliable basis for simulating surface phenomena and gives the theoretical analysis in high-energy electron reflection a more solid foundation.

In general, the BMCR method only provides a new apparatus for solving a problem rather than the solution to the problem. From our point of view, there are still two very basic problems in high-energy electron reflection which remained unanswered or incompletely answered:

(i) The source of two-dimensional RHEED patterns. So far, numerical analyses using the Bloch-wave method or multislice method or the BMCR method are all only consistent with semicircular RHEED patterns, most of which were recorded by using a special RHEED camera under the UHV condition (Siegel & Menadue, 1967; Ino, 1977, 1980).

(ii) The true source of surface resonance phenomena.

These two problems may be the keys to open the door to more-informative RHEED patterns and REM images. The BMCR method obviously could play a role in further studies in this field.

This work was supported by the National Science Foundation through Northwestern University Materials Research Center, Grant No. DMR 85-20280.

References

BETHE, H. (1928). *Ann. Phys. (Leipzig)*, **87**, 55-129.
BRITZE, K. & MEYER-EHMSEN, G. (1978). *Surf. Sci.* **77**, 131-141.
COLELLA, R. (1972). *Acta Cryst.* A**28**, 11-15.
COWLEY, J. M. & PENG, L. M. (1985). *Ultramicroscopy*, **16**, 59-68.
DAIMON, H. & INO, S. (1985). *Surf. Sci.* **164**, 320-326.
FESHBACH, H. (1958). *Ann. Phys. (Leipzig)*, **5**, 357-390.
FUJIMOTO, F. (1959). *J. Phys. Soc. Jpn*, **14**, 1558-1568.
ICHIMIYA, A. (1983). *Jpn. J. Appl. Phys.* **22**, 176-180.
INO, S. (1977). *J. Appl. Phys. Jpn*, **16**, 891-908.
INO, S. (1980). *J. Appl. Phys. Jpn*, **19**, 1277-1290.
KATO, N. (1952). *J. Phys. Soc. Jpn*, **7**, 397-414.
KIKUCHI, S. & NAKAGAWA, S. (1933). *Sci. Pap. Inst. Phys. Chem. Res. Tokyo*, **21**, 256-265.
KOHRA, K., MOLIERE, K., NAKANO, S. & ARIYAMA, M. (1962). *J. Phys. Soc. Jpn*, **17**, Suppl. B-II, 82-85.
MA, Y. (1990). *Acta Cryst.* submitted.
MA, Y. & MARKS, L. D. (1989). *Acta Cryst.* A**45**, 174-182.
MA, Y. & MARKS, L. D. (1990). *Acta Cryst.* A**46**, 11-32; erratum: *Acta Cryst.* (1990). A**46**, 626.
MCRAE, E. (1966). *J. Chem. Phys.* **45**, 3258-3276.
MCRAE, E. A. & CALLDWELL, C. W. (1976). *Surf. Sci.* **57**, 63-76.
MCRAE, E. G. (1979). *Rev. Mod. Phys.* **5**, 357-390.
MAKSYM, P. A. & BEEBY, J. L. (1981). *Surf. Sci.* **110**, 423-438.
MAKSYM, P. A. & BEEBY, J. L. (1982). *Appl. Surf. Sci.* **11/12**, 663-676.
MARKS, L. D. & MA, Y. (1988). *Acta Cryst.* A**44**, 392-393.
MARKS, L. D. & MA, Y. (1989*a*). *Ultramicroscopy*, **29**, 183-191.
MARKS, L. D. & MA, Y. (1989*b*). *Ultramicroscopy*, **31**, 241-244.
MENADUE, J. F. (1972). *Acta Cryst.* A**28**, 1-11.
MIYAKE, S. & HAYAKAWA, K. (1966). *J. Phys. Soc. Jpn*, **21**, 363-378.
MIYAKE, S., KOHRA, K. & TAKAGI, M. (1954). *Acta Cryst.* **7**, 393-401.
MOON, A. R. (1972). *Z. Naturforsh. Teil A*, **27**, 390-395.
PENG, P. M. & COWLEY, J. M. (1986). *Acta Cryst.* A**42**, 545-552.
PENG, P. M. & COWLEY, J. M. (1988). *Surf. Sci.* **199**, 609-622.
SIEGEL, B. M. & MENADUE, J. F. (1967). *Surf. Sci.* **8**, 206-216.
SOMORJAI, G. A. (1981). *Chemistry in Two Dimensions, Surfaces*, 1st ed., p. 126. Ithaca: Cornell Univ. Press.
TURNER, P. S. & COWLEY, J. M. (1981). *Ultramicroscopy*, **6**, 125.
WANG, Z. L., LU, P. & COWLEY, J. M. (1987). *Ultramicroscopy*, **23**, 205-222.
WHELAN, M. J. & HIRSH, P. B. (1957). *Philos. Mag.* **2**, 1121-1142, 1303-1324.
ZHAO, T. C., POON, H. C. & TONG, S. Y. (1988). *Phys. Rev. B*, **38**, 1172-1182.
ZHAO, T. C. & TONG, S. Y. (1988). *Ultramicroscopy*, **26**, 151-160.

Acta Cryst. (1990). A**46**, 606-619

Direct Solution of Continuous Densities Given the Fourier Magnitudes

BY ROBERT W. HARRISON

Crystallography Laboratory, National Cancer Institute - FCRF, PO Box B, Frederick, MD 21701, *USA*

(*Received* 12 *September* 1989; *accepted* 12 *February* 1990)

Abstract

In order to apply direct methods routinely to macromolecular crystals it will be necessary to generate a non-atomic theory which is applicable to continuous densities. Reformulation of the 'phase problem' in terms of deconvoluting an autocorrelation function or Patterson synthesis reduces the problem from a theoretically intractable transcendental problem to a system of simultaneous quadratic equations. These quadratic equations may, in principle, always be solved by conjugate direction search techniques. The phase problem is shown to be a class P problem, admitting a deterministic solution in polynomial time. Two algorithms are presented with running times proportional to N^2_{points} and $N_{\text{points}} \log N_{\text{points}}$ per step. These algorithms are a pixel-by-pixel search and a conjugate gradients search. When the data are exact and complete the Fourier magnitudes are readily inverted by them to find the image. An example with real data, from a 15mer of DNA, is also shown.

Introduction

The phase problem in crystallography occurs because it is only possible, in general, to measure the amplitude of the diffracted X-ray. A great deal of effort has gone into various methods for overcoming this problem. Experimental means like isomorphous replacement and anomalous scattering (Blow & Crick, 1959; Watenpaugh, 1985; Hendrickson, Smith & Sheriff 1985) for macromolecules, as well as theoretical approaches like direct methods (Karle & Hauptman, 1950; Ladd & Palmer, 1980) for small molecules have been developed to find useable values for the phases. These have been successful, but the general solution to the phase problem has remained elusive. In particular, it has been very difficult to invert numerically the observed magnitudes and obtain the electron density when the density neither is composed of a small number of atoms, nor diffracts to high resolution. This is typically the case with macromolecular structures.

0108-7673/90/070606-14$03.00